

1 **Methanol on the rocks: Green rust transformation promotes the oxidation of** 2 **methane**

3 Orion Farr^{a,b}, Nil Gaudu^b, Gregoire Danger^c, Michael J. Russell^d, Daniel Ferry^a, Wolfgang
4 Nitschke^b, Simon Duval^b

5 a. Aix-Marseille Univ, CNRS, CINaM, F-13009, Marseille, France

6 b. CNRS, BIP (UMR 7281), Aix Marseille Univ, Marseille, France

7 c. Aix-Marseille Univ, CNRS, PiiM, F-13013, Marseille, France

8 d. Dipartimento di Chimica, Università degli Studi di Torino, Italy

9 *Corresponding author: Orion Farr

10 Email: orionfarr@gmail.com

11

12 ***I. Abstract:***

13 Shared coordination geometries between metal ions within reactive minerals and enzymatic metal cofactors
14 hints at mechanistic and possibly evolutionary homology between particular abiotic chemical mineralogies
15 and biological metabolism. The octahedral coordination of reactive Fe^{2+/3+} minerals such as green rusts,
16 endemic to anoxic sediments and the early Earth's oceans, mirrors the di-iron reaction center of soluble
17 methane monooxygenase (sMMO), responsible for methane oxidation in methanotrophy. We show that
18 methane oxidation occurs in tandem with the oxidation of green rust to lepidocrocite and magnetite,
19 mimicking radical mediated methane oxidation found in sMMO to yield not only methanol but also
20 halogenated hydrocarbons in the presence of seawater. This naturally occurring geochemical pathway for
21 CH₄ oxidation elucidates a previously unidentified carbon cycling mechanism in modern and ancient
22 environments and reveals clues into mineral-mediated reactions in the synthesis of organic compounds
23 necessary for the emergence of life.

24 ***II. Introduction:***

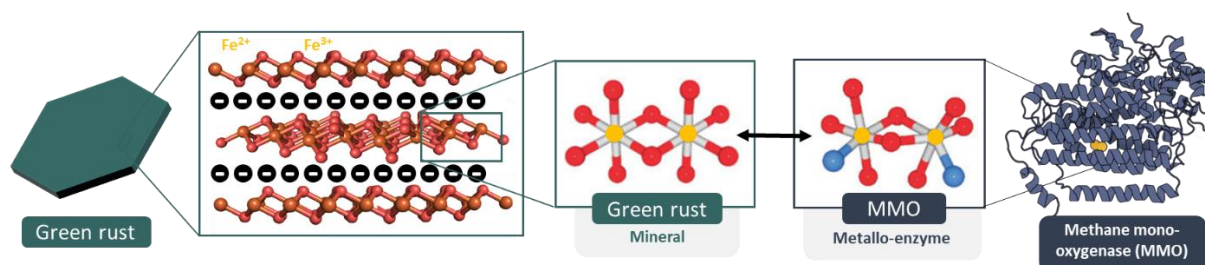
25 Methane (CH₄), although currently present at only 1.9 ppm, is the major heat-trapping greenhouse gas in
26 terms of its radiative forcing effect, having 80x the effect of CO₂ [1]. Anthropogenic emissions of CH₄ now
27 outweigh natural sources produced via biotic (organic degradation) and abiotic (serpentinization, mantle
28 degassing) mechanisms. Natural sinks exist for CH₄ but are insufficient to offset growing anthropogenic
29 output. In the biosphere, CH₄ is readily oxidized by methanotrophs, yielding methanol (MeOH), a key
30 metabolic intermediate towards biomass formation [2,3]. In many species this metabolism employs the
31 enzyme soluble methane monooxygenase (sMMO) to react CH₄ with oxygen (O₂), N₂O, or H₂O₂ over an
32 ephemeral di-Fe(IV) intermediate reaction center to achieve the conversion of CH₄ to MeOH [4]. A similar
33 reaction mechanism takes place within man-made catalysts where Fe(IV) reaction centers embedded within
34 mineral scaffolds are used to convert CH₄ to value-added products [5–7]. The oxidation state Fe(IV), which

35 is only ephemeral in nature, is crucial to the energetically demanding partial oxidation of CH₄ for biological
36 and industrial purposes [7,8].

37 Methane is thought to have had an even larger role in climate regulation during the Hadean-Archean Eons
38 4.4 to 3.2 Ga, where the estimated atmospheric abundance of greenhouse gasses like CH₄, CO₂, and N₂O
39 were orders of magnitude greater than modern, supplying ample CH₄ for the proliferation of primitive
40 methanotrophs [9,10]. This anaerobic metabolism, along with various others, dominated the biosphere until
41 the emergence of oxygenic photosynthesis during the great oxidation event (GOE) [11].

42 Of pertinence to the experiments and outcomes reported herein, the octahedral di-iron reaction center
43 structure of sMMO shares similar coordination geometry to the octahedral di-valent iron lattice coordination
44 in green rusts (GR) (Figure 1) [12]. This group of naturally forming, metastable, reactive, layered double
45 hydroxide (LDH) minerals are known for their redox capabilities in carrying out the reduction of metals (e.g.,
46 Cu, As, U), inorganic compounds (e.g., NO₃⁻, ClO₄⁻), and organic compounds (e.g., CT, TCE, TCM [13–18].
47 GR's unique structure consists of a charged octahedrally coordinated bilayer of multivalent cations (e.g.,
48 Fe, Ni, Mg, Al) sandwiching interchangeable anions (e.g., CO₃²⁻, HCOO⁻, Cl⁻, SO₄²⁻) [19]. The mineral reacts
49 with oxygen, radicals, and temperature to undergo pH- and eH-dependent transformations into other
50 reactive minerals, namely magnetite and lepidocrocite, playing a yet unquantified role in the geochemical
51 cycling of sub-oxic subsurface environments [20–22]. Of note is its proposed role in marine nutrient and
52 metal geochemical cycling prior to the GOE at ~ 2.5Ga [23,24], and its hypothesized suitability as an “abiotic
53 enzyme” linking geochemical proto-metabolism with the evolution of enzymatic biochemistry prior to the
54 emergence of life [12,25–27].

55 A. Figure 1. Diagram of similarities between metal ion coordination in GR and sMMO



58 **Figure 1.** A diagram comparing the structural similarities between GR and sMMO. From left to right, an
59 illustration of a single GR crystal, the crystal's cation and anion LDH structure, the octahedral
60 coordination of iron (yellow) and oxygen (red) atoms in GR, the analogous atomic structure of the MMO
61 reaction center (nitrogen = blue), and a model of the enzyme MMO.

62 The di-iron structure present in sMMO and synthetic catalysts is known to be the key site essential in the
63 oxidation of methane. Thus, the presence of an analogous structure in GR suggests that it also has the

64 potential to catalyze methane oxidation. In this study, we experimentally demonstrate the viability of this
65 proposed analogous catalytic behavior by reacting green rust with CH₄ and O₂ to produce significant
66 quantities of MeOH and halogenated organics. These results uncover previously unrecognized redox
67 reactions with GR and the carbon cycle, yielding significant environmental implications to the modern and
68 ancient Earth.

69 **III. Methods:**

70 1.1 Mineral synthesis

71 Three GR species and their transformation products were synthesized following procedures outlined in
72 Ruby (2003) and Bocher (2004). The main species of GR studied was a green rust intercalated with the
73 carbonate anion (GRCO₃) and its synthesis is described below. Synthesis for GRSO₄ and GRCl is detailed
74 in the supplementary section S1.

75 A concentrated stock solution of simulated seawater containing 150 mM FeCl₂·H₂O, 50 mM FeCl₃, 50 mM
76 of MgCl, and 400 mM of NaCl was prepared using deoxygenated ultra-purified water (milli-Q) and purged
77 with N₂ gas for 30 minutes in a sealed 125 mL reactor vial. A solution of 300 mM NaOH and 30 mM Na₂CO₃
78 was then injected into the reactor via a N₂-purged needle syringe and the mixture was gently shaken. A
79 dark green precipitate formed which was then confirmed to be GRCO₃ via powder X-ray diffraction (section
80 d). The Fe concentration of these GR stock suspensions were 200 mM and final pH was ~7.

81 1.2 Methane oxidation reactions

82 The pressurized reactions took place inside a 200 ml Parr autoclave reactor pressurized to 0, 1, 10, 30, 50
83 bar CH₄ (Linde Gas 99.99%), 0-3 bar O₂ (Linde), 1 bar NO (Linde Gas 5%), at 25°C. Within the reactor 20-
84 100 ml glass vials with stirrers, butyl or screw top caps, and needle-perforated septa were used to contain
85 the replicate mineral suspensions. These vials were then removed and stored under anoxic conditions
86 before their headspaces were analyzed using GC-MS.

87 1.3 Headspace Analysis

88 GC gas chromatography coupled to an ISQ mass spectrometer (ThermoFisher Scientific). The sampling
89 was performed by headspace (HS) using an RSH auto-sampler (ThermoFisher Scientific). 5 mL of each
90 sample was deposited on a 20 mL HS vial with screwtop PTFE septas. Each vial was then incubated during
91 6 min at 55°C under agitation. The HS sampling was performed by collecting 2 mL of the gas phase. It was
92 then injected into the GC via an injector at 250°C, a split at 10 mL/min and a column flow of 1.1 mL/min.
93 The column was a Stabilwax-DA from Restek (length 30m, diameter 0.25 mm, film thickness 0.5µm).
94 Analyses were performed with the temperature gradient that starts with a 1 min isotherm at 35°C and
95 proceeds with a gradient at 25°C/min up to 220°C ending with a 2 min isotherm. The detection was
96 performed with the MS in full scan or SIM mode using an electron impact ionization at 70eV. MS transfer

97 line and ion source temperatures were set at 250°C. For the full scan analyses, the m/z range was 20-300
98 au, meanwhile for the SIM m/z 31 and 84 were isolated for MeOH and TCM identification (Figure S6).

99 4.4 Mineral characterization

100 Mineral transformation over the course of the reaction was monitored using X-ray diffraction (XRD),
101 transmission electron microscopy (TEM), and scanning electron microscopy (SEM). Samples were
102 centrifuged, decanted, and dried under a stream of N₂ gas. For XRD analysis glycerol was added prior to
103 analysis to prevent oxidation and the paste was transferred into a glass ampule for XRD analysis in a
104 Rigaku RU 200BH diffractometer with Cu anode ($\lambda = 1.5418\text{\AA}$), scanning from 2 theta values of 2-80
105 degrees. For TEM analysis, an aliquot of dried mineral was deposited on a copper grid coated with a holey
106 carbon film (AGAR Scientific, S147-3). Grids were then transferred to a Jeol-JEM2010 electron microscope
107 operated at 200 kV and GR particles were observed in bright field mode. For SEM analysis, an aliquot of
108 dried mineral was deposited on an aluminum sample holder and then transferred to a Jeol JSM-7900F
109 electron microscope and analyzed using accelerating voltages ranging from 5 to 15 kV.

110

111 **IV. Results:**

112 The pressurization of GR with CH₄ and O₂ resulted in the production of MeOH along with various
113 other compounds, including trichloromethane (TCM) and dichloromethane (DCM). Various conditions
114 were tested to optimize the yield of MeOH.

115

116

117

118

119

120

121

122

123

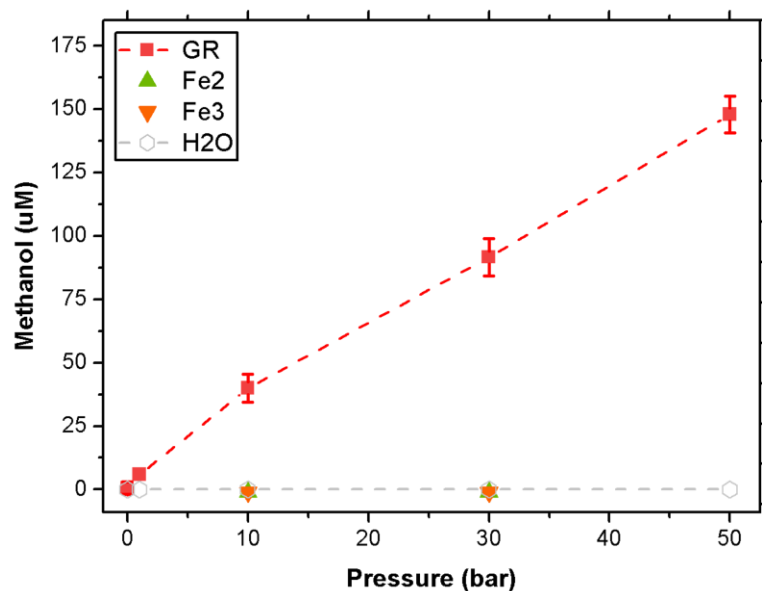
124

125

126
127

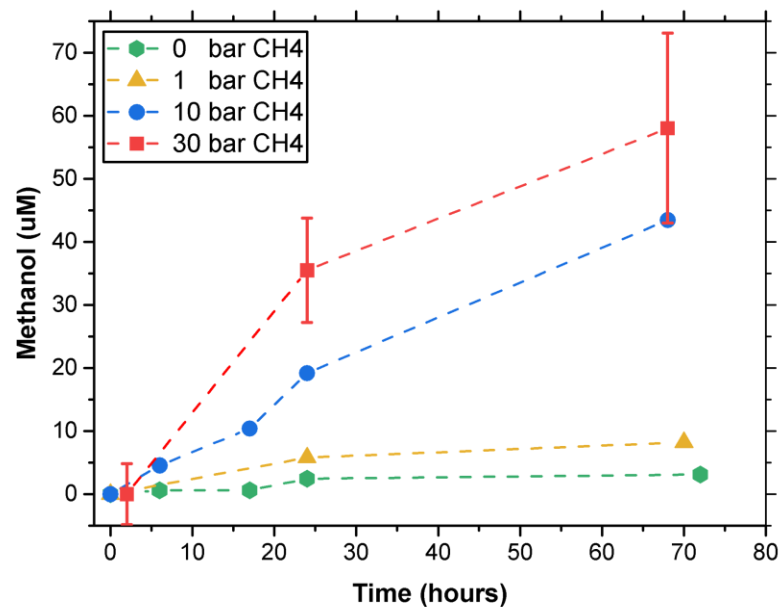
b. [Figure 2 – Effect of pressure and time on methanol concentration]

A



128

B



129

130 **Figure 2:** Graph A displays methanol concentrations at given CH₄ partial pressure following 24 hours of
131 reaction time in solutions containing GRCO₃, FeCl₂, FeCl₃, and H₂O. Graph B displays a related set of
132 experiments conducted at [Fe] = 30 mM, showing methanol production over time.

133

134 Figure 2a shows MeOH concentrations in solutions of GRCO_3 ($[\text{Fe}]=200\text{mM}$) following 24 hours of
135 pressurization to 0, 1, 10, 30, and 50 bars of CH_4 mixed with 0.2 bar O_2 . There is a significant increase in
136 MeOH concentration with increasing pressure. At 10 bar CH_4 , solutions of GRCO_3 with a total $[\text{Fe}]=200\text{mM}$
137 yield $30\mu\text{M}$ MeOH which increases 5-fold with a corresponding 5-fold increase to 50 bar CH_4 . Thus MeOH
138 concentration increases with a linear relationship with pressure [$y=(2.88\text{E}-6)x+5.30\text{E}-6$]. Multiple
139 concentrations were examined and the relationship between $[\text{MeOH}]/[\text{Fe}]$ is compared (Supplementary
140 figure 5). MeOH is only detected with GR in the initial solution, as solutions containing FeCl_2 , FeCl_3 , or H_2O
141 did not produce detectable levels of MeOH under the same conditions. No MeOH is detected without the
142 added oxidants. Substitutes for O_2 , NO and H_2O_2 , were tested and found to produce products of CH_4
143 oxidation (Supplementary figure 7).

144 Figure 2b shows the production of MeOH over time in solutions of GRCO_3 ($[\text{Fe}]=30\text{mM}$) with partial
145 pressures of CH_4 from 0 to 30 bar mixed with 0.2 bar O_2 . These experiments were conducted at lower
146 concentrations of Fe than Figure 2 (30 vs 200mM). No MeOH is detected in solutions of GR not exposed
147 to CH_4 . With 1 bar CH_4 there is a mild increase to $\sim 5\mu\text{M}$ of MeOH. At 10 bars CH_4 there is an increase from
148 0 to $\sim 40\mu\text{M}$ of MeOH by 80 hours. At 30 bar of CH_4 we show an increase from 0 to $\sim 55\mu\text{M}$ of MeOH by 68
149 hours of reaction time. The addition of 0.2 bar O_2 and subsequent MeOH production resulted in changes to
150 solution pH, which was recorded to drop from an initial value of 7 to 6 by 24 hours and 5 by ~ 70 hours.
151 Additional experiments were attempted with 1 bar O_2 and 10 bar CH_4 , leading to rapid mineral
152 transformation yet no measurable MeOH production.

153 Coinciding with MeOH production was the production of various organic compounds produced in μM
154 quantities. The most prevalent compounds detected other than MeOH were halogenated organics, mainly
155 TCM and DCM (Supplementary figure 2). The concentration of TCM and DCM increased in response to
156 increased pressure, however DCM was the primary organohalogen detected at higher pressures (30 bar)
157 versus TCM dominating at lower pressures. Trace amounts of TCM were also detected without the
158 presence of O_2 in aged GRCO_3 solutions exposed to CH_4 . However, TCM was also produced in solutions
159 of FeCl_2 when exposed to CH_4 . Other organic products were produced but were not easily replicated and
160 thus were not quantified: these compounds included $\text{C}_1\text{-C}_{12}$ hydrocarbons, butanal, pentanal,
161 paraformaldehyde, acetaldehyde, and dimethyl ether.

162

163

164

165

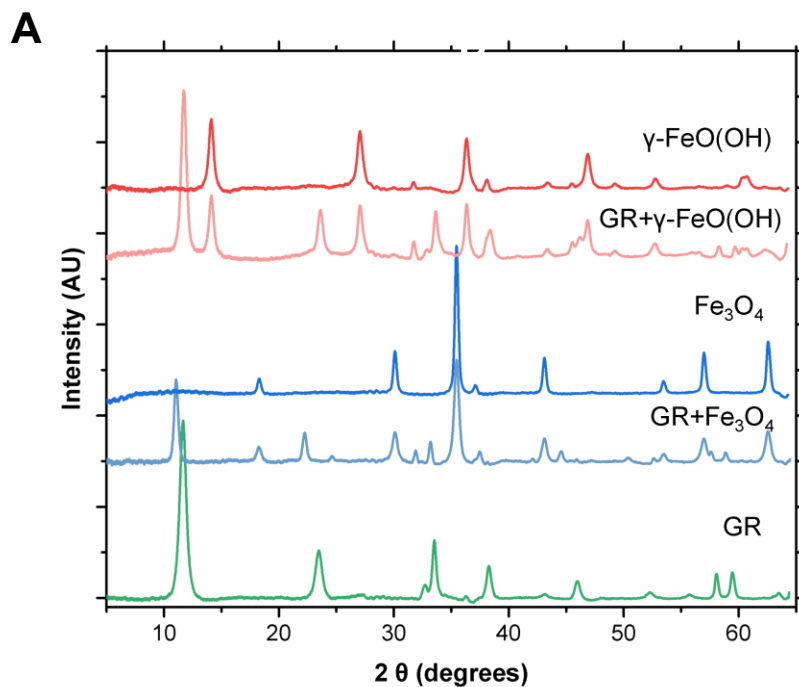
166

167

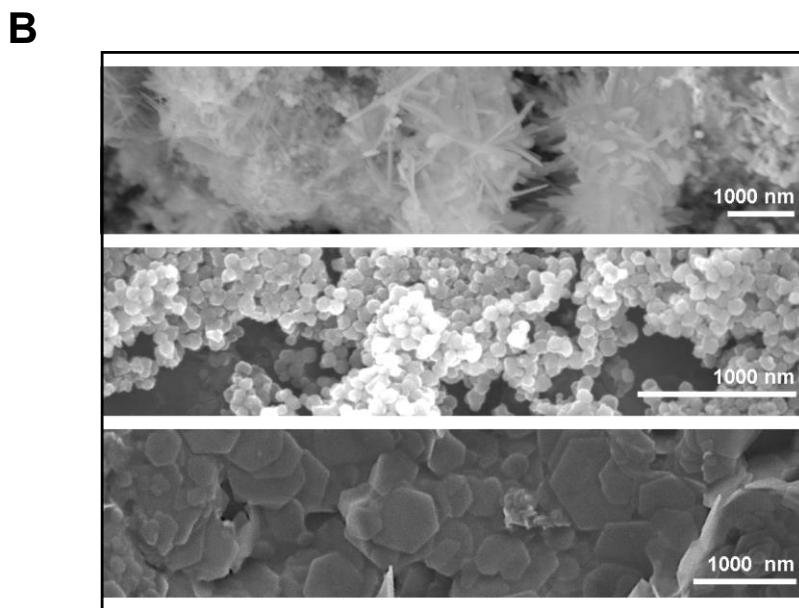
168

169

c. Figure 3-Transformation XRD and TEM]



170



171

172 **Figure 3** – Section A displays the XRD chromatograms of GR and its partial and full transformation
173 products magnetite (Fe_3O_4) and lepidocrocite (γ -FeO(OH)) following the exposure to pressurized CH_4/O_2
174 atmospheres. Section B displays SEM images of the adjacent pure mineral phases.

175

176

177

178 GR undergoes transformation to two mineral phases following the exposure to pressurized CH₄ and O₂
179 mixtures, oxidizing to either magnetite (Fe₃O₄) or lepidocrocite (γ-FeO(OH)) according to XRD (Figure 3a).
180 The presence of O₂ (0-1 bar) at the start of the reaction resulted in different transformation product yields,
181 with increased O₂ selecting for γ-FeO(OH) over Fe₃O₄. Full transformation takes place within 68 hours of
182 reaction. SEM (Figure 3b) images show distinct transformation from GR's characteristic 10 to 500 nM
183 hexagonal platelets, through an intermediate phase with hexagonal plates studded with <100 nM spheroid
184 assemblages or <100nm irregular acicular crystals, to a fully transformed phase with only spheroids or
185 acicular crystals. The transformation of GR results in a decrease from an initial average pH of 7 to 5.

186 **v. Discussion:**

187 Our experiments show that the oxidative transformation of GR in the presence of CH₄ results in the oxidation
188 of CH₄, to a variety of products. In section a, we discuss the analysis of MeOH, as well as the other
189 compounds (e.g. TCM, DCM) detected in significant quantities.

190 a. The concurrent oxidation of green rust and methane

191 The production of MeOH at various pressures and over time is depicted in figure 2, showing significant
192 quantities are produced in solutions of GR pressurized to 1-50 bar over 60 hours, given the initial presence
193 of 0.2 bar of O₂ at the start of the experiment. However, in the absence of oxygen, the introduction of CH₄
194 to GR resulted in little to no MeOH production. Substitutes for O₂ were tested, using H₂O₂ (Supplementary
195 figure 5) and NO (Supplementary figure 7) in separate experiments, yielding MeOH and butanal
196 respectively. The presence of a sufficient oxidant is therefore implicated in the successful oxidation of
197 methane using GR.

198 Increasing CH₄ pressure resulted in a linear increase in MeOH concentration over a range of [Fe] (200,
199 100, 30 mM). Increasing the concentration of Fe results in higher yield of MeOH, however the efficiency of
200 the production of MeOH/Fe falls dramatically (Supplementary figure 5). GR's affinity to hydrophilic O₂ and
201 as well as radical scavenging likely dominates surface interactions versus hydrophobic gases like CH₄. The
202 reaction rate is thus dependent on how much CH₄ is in contact with the mineral surface, which is controlled
203 by the concentration of dissolved CH₄ in solution (Figure 2). CH₄ solubility is controlled by pressure and
204 chloride concentration due to CH₄'s low solubility in distilled water at STP – solubility increases 42% from
205 1 to 50 bars but is decreased by 20% with the addition of 0.4 M Cl⁻ [30]. The solubilization of CH₄ is one
206 route for aqueous mineral reactions, however within pore spaces common to sediments and hydrothermal
207 systems where this reaction would occur, direct contact with trapped CH₄ bubbles would offer a more direct
208 mineral-to-gas interface, increasing the reaction rate.

209 The substitution of interlayer anions is known to affect GR reactivity [31] and our investigation of Cl⁻, CO₃²⁻
210 , and SO₄²⁻ (Supplementary figure 4) shows an unexpected trend in reactivity with CO₃²⁻>Cl⁻>SO₄²⁻. With

211 prior work in GR, redox reactions involving the various anions show clear preference for Cl^- and SO_4^{2-} over
212 CO_3^{2-} reactions [19]. As the GRCO_3 and GRCl solutions were conducted in simulated seawater, a mixed
213 interlayer phase of $\text{CO}_3^{2-}+\text{Cl}^-$ could conceivably be responsible for increased reactivity towards CH_4
214 oxidation. The increased MeOH production could also be linked to the reduction of interlayer bound CO_3^{2-}
215 during the reaction [32].

216 The production of halogenated organic molecules was observed (Supplementary figure 2): GR appears to
217 catalyze CH_4 chlorination as TCM and DCM are products in solutions containing GR and NaCl. GR and
218 magnetite are known to reduce halogenated organics [33], which may explain the preference for DCM over
219 TCM at higher pressure. Given time, this reduction should continue to methyl chloride and CH_4 . Chlorine
220 could likely be replaced by other environmentally relevant halogens such as iodine or bromine, indicating a
221 general abiotic link between Fe redox and halogen cycling in the environment.

222 MeOH was not detected in parallel experiments using solutions of H_2O , NaCl, or FeCl_2 , or FeCl_3 in place of
223 GR. Since no MeOH is formed without GR or without O_2 , GR must be producing a short-lived reactant
224 during oxidation necessary for the reaction to proceed over GR or its oxide transformation products; ferric
225 green rust, magnetite, or lepidocrocite.

226

227 b. Radicals and Fe(IV) mediated oxidation mechanism

228 The presence of radicals and Fe(IV) oxidation states are routinely implicated in CH_4 oxidation research as
229 a main mechanism for achieving the energetically difficult partial oxidation of methane over transition metal
230 bearing mineral catalysts such as zeolites [6,7]. These high surface area aluminosilicate minerals bear Fe
231 (II-III) reaction sites which readily react with oxidative species such as O_2 , H_2O_2 , N_2O , UV, or radicals to
232 create short lived reactive Fe(IV) oxidation states which can effectively conduct CH_4 oxidation [5,7,34]. This
233 Fe(IV) state is likewise responsible for CH_4 oxidation in microbial methanotrophy, where the enzyme sMMO
234 uses oxidant-activated Fe(IV) reaction centers to transform CH_4 to MeOH [4]. Correspondingly, in GR, it's
235 oxidative transformation is known to produce a significant amount of hydroxyl radicals, H_2O_2 , and Fe(IV)
236 sites [35,36] which have been observed to promote the degradation of complex organic molecules [37,38].

237 Given the known relationship between radical production, Fe(IV) sites, and methane oxidation, we propose
238 that GR mediates CH_4 oxidation via radical mediated oxidation pathway over short-lived Fe(IV) sites in a
239 manner similar to sMMO [8] or Fe-ZSM zeolites [6]

240 To further test this hypothesis, we replicated the experimental conditions for GRCO_3 at 1 bar CH_4 and
241 replaced O_2 with 1 mM of H_2O_2 which yielded a significant amount of MeOH even without high pressures
242 (Supplementary figure 5). This indicates the reaction is dependent on the interaction between hydroxyl
243 radicals, iron, and CH_4 [39]. Furthermore, MeOH serves as a radical scavenger resulting in its own oxidation
244 to formaldehyde (which was detected), formate, and CO_2 [40]. The production of organohalogen in the

245 presence of Cl⁻ anions, likely through a radical chlorination pathway [41], adds further evidence to the
246 radical-based hypothesis. In this case, the Cl⁻ radical ion substitutes for the hydroxyl radical to oxidize CH₄
247 yielding methyl chloride (MC), DCM, and TCM, instead of MeOH, which was observed in our experiments.

248 c. Implications

249 The discovery of a naturally occurring mineral-based mechanism for CH₄ oxidation is novel and hints at
250 large scale geochemical processes that have been overlooked with past research.

251 *Feasibility and environmental relevance*

252 The conditions simulated within the pressure reactor (GR in contact with pressurized CH₄) provided optimal
253 conditions for the reaction in addition to serving as an analogue to environmental conditions where GR
254 could conceivably interact with sources of CH₄ at depth. GR has been isolated in deep anoxic ferruginous
255 lakes [21] and is speculated to form at hydrothermal vents and [42] where oxygen-poor hydrothermal fluids
256 meet cold oxygen-rich sea water. In both locales, abiotic and biotic sources of CH₄, pressurized at depths
257 (e.g. 100 m depth = 10 bar pressure) would fall within the range of conditions we tested. For environments
258 closer to STP, such as wetland sediments, soils, and ground water, our experimental results still
259 demonstrate GR's reactivity towards CH₄ oxidation, albeit one accelerated by pressure. We observed both
260 MeOH and halogenated organics at 1 bar CH₄, though in low concentrations, indicating that mineral based
261 CH₄ oxidation will take place even under STP. The discovery of naturally occurring mineral-based
262 mechanism for CH₄ oxidation is novel and hints at global geochemical processes that have been previously
263 overlooked.

264 *Implied role of green rust in carbon and halogen cycling in modern environments*

265 Green rusts are well studied for their use in the degradation of organohalogen pollutants in the environment
266 [43–46], however they have never been linked to organohalogen formation via CH₄ oxidation. Recent
267 observations revealed that salt plains, rainforests, and soils are the source of abiotic emissions of
268 chloromethanes [47–51]. Of note is the isotopic fractionation of some of these signatures, implying an
269 abiotic source [50]. As mentioned previously, GR is common in these types of waterlogged environments
270 [52] and within anoxic regions of stratified bodies of water and rivers with high iron content [21,53]. In soils,
271 Fe is already known to halogenate decaying organic matter[47], the direct oxidation of CH₄ has not yet been
272 observed in the environment. Our experiments show that it is feasible for GR to be oxidatively transformed
273 to reactive Fe-oxides in the presence of CH₄, thus catalyzing CH₄ oxidation, providing a source of these
274 chloromethanes, as well as serving as a potential abiotic sink for modern CH₄. As CH₄, halomethane, and
275 halogen flux greatly affect climate forcing [54] uncovering the role reactive minerals play in these cycles
276 may help constrain their input over climate change. Overall, the further study of these environments should
277 take care to identify O₂-sensitive minerals like GR, to understand the extent of their influence over the
278 geochemical cycling of carbon and halogens.

279 *Methane oxidation on the ancient Earth*

280 Abiotic CH₄ oxidation may have played a greater role in the deep past as long periods of ferruginous oceans
281 characterized the Archean (4-3.5 Ga) and Proterozoic (3.5-2 Ga) eons [24,55,56]. During these periods
282 GRs are thought to have been abundant and likely shepherded marine geochemistry at the interface
283 between land, air, and sea [21,24,57]. Prior to the GOE and the subsequent proliferation of O₂ in marine
284 environments; geochemically generated radical species [39,58–60], thermochemical processes [22,61],
285 nitrogen oxides [18,62], and nitrogen oxyanions [63,64], may have served as potential surrogates for the
286 oxidation of GR and thus CH₄, creating a CH₄ sink within the ancient Archean oceans.

287 As halomethanes exert strong influences over the greenhouse effect [54], the effect of their production by
288 a GR saturated ocean on the Archean climate is currently unstudied. As such, the detection of exoplanet
289 halomethane signatures may not necessarily indicate the presence of life, as was recently suggested [65].
290 However, as life is thought to have emerged sometime in the late Hadean to early-Archean, the oxidation
291 of abundant CH₄ [10] to more biochemically accessible compounds such as MeOH, hydrocarbons, and
292 halogenated organics may have played important roles both before and after its emergence.

293 More specifically, our results strengthen an emergence-of-life hypothesis that invokes a pathway for GR-
294 mediated protocell synthesis [3,12,25,26], where hydrothermal CH₄ is oxidized to multi-carbon compounds
295 within GR-saturated mineral membranes precipitated at the redox boundary between reducing alkaline vent
296 effluent and oxidizing acidic ocean water – the type of disequilibria considered to have driven life into being
297 [66]. Just as in the biological metabolism of methanotrophy, methane would thereby serve both as a
298 feedstock for production of organics and as a source of a cascade of increasingly reducing electrons derived
299 from the further oxidation of MeOH, formaldehyde etc, as discussed in [3,67]. As pointed out previously,
300 such entropy-decreasing processes are prerequisites for thermodynamically meaningful emergence-of-life
301 scenarios [68]. Given the similarities between sMMO's di-iron reaction center and GR's atomic lattice
302 coordination, a proposed evolutionary link between minerals and enzymes is suggested [69]. Because GR
303 has a uniquely versatile structure which allows for chemical exchange; integrating several essential metals
304 (e.g., Co, Ni, Zn, Mo) and anionic (e.g., NO³⁻, formate, linear carbon chain) species, it is suggested that its
305 bilaterally active interlayers served as sites for organic synthesis [32] at early submarine alkaline
306 hydrothermal vents, and that these interlayers also compartmentalized and guided the free-energy
307 converting proto-metabolic processes which led to the emergence of life [12,25,26].

308 **vi. Conclusion:**

309 We demonstrate that the oxidative transformation of green rust in the presence of methane yields methanol,
310 along with organohalogens and various other organic compounds. This newly discovered behavior implies
311 the existence of previously undetected links between iron, carbon, and halogen redox cycling in the
312 environment mediated by reactive minerals. Furthermore, the reaction mechanism is likely analogous to
313 the radical-promoted oxidation of CH₄ mediated by the enzyme sMMO, inviting further research into the

314 relationship between the evolution of primitive microbial metabolisms and the abiotic geochemical
315 processes that preceded them.

316 **vii. Acknowledgements:**

317 This work received support from the French Government under the France 2030 investment plan, as part
318 of the initiative d'Excellence d'Aix Marseille Université (A*MIDEX -AMX-21-PEP-039) as well as a grant
319 from the French Agence Nationale pour la Recherche (ANR-22-CE30-0035-01).

320 We thank Vasile Heresanu for performing XRD measurements, Alexandre Altié and Damien Chaudanson
321 for SEM/TEM support, Frederic Brunel for lending us the pressure reactor, and Olivier Grauby for helpful
322 discussions on green rust.

323 **viii. Authors contributions**

324 OF designed and performed experiments. OF, NG, GD, MR, DF, WN, SD contributed to the manuscript.

325 **ix. Conflict of interest**

326 The authors note no conflict of interest.

327 **x. References:**

- 328 1. Jackson RB *et al.* 2021 Atmospheric methane removal: A research agenda. *Philosophical*
329 *Transactions of the Royal Society A: Mathematical, Physical and Engineering Sciences* **379**.
330 (doi:10.1098/rsta.2020.0454)
- 331 2. Chistoserdova L, Vorholt JA, Thauer RK, Lidstrom ME. 1998 C1 Transfer Enzymes and
332 Coenzymes Linking Methylophilic Bacteria and Methanogenic Archaea. *Science (1979)* **281**, 99–
333 102. (doi:10.1126/science.281.5373.99)
- 334 3. Russell MJ, Nitschke W. 2017 Methane: Fuel or Exhaust at the Emergence of Life? *Astrobiology*
335 **17**, 1053–1066. (doi:10.1089/ast.2016.1599)
- 336 4. Kopp DA, Lippard SJ. 2002 Soluble methane monooxygenase: activation of dioxygen and
337 methane. *Curr Opin Chem Biol* **6**, 568–576. (doi:10.1016/S1367-5931(02)00366-6)
- 338 5. Nizova G V., Süß-Fink G, Shul'pin GB. 1997 Catalytic oxidation of methane to methyl
339 hydroperoxide and other oxygenates under mild conditions. *Chemical Communications* , 397–398.
340 (doi:10.1039/a607765j)
- 341 6. Starokon E V., Parfenov M V., Arzumanov SS, Pirutko L V., Stepanov AG, Panov GI. 2013
342 Oxidation of methane to methanol on the surface of FeZSM-5 zeolite. *J Catal* **300**, 47–54.
343 (doi:10.1016/j.jcat.2012.12.030)
- 344 7. Dummer NF *et al.* 2023 Methane Oxidation to Methanol. *Chem Rev* **123**, 6359–6411.
345 (doi:10.1021/acs.chemrev.2c00439)
- 346 8. Banerjee R, Proshlyakov Y, Lipscomb JD, Proshlyakov DA. 2015 Structure of the key species in
347 the enzymatic oxidation of methane to methanol. *Nature* **518**, 431–434. (doi:10.1038/nature14160)

- 348 9. Arney G, Domagal-Goldman SD, Meadows VS, Wolf ET, Schwieterman E, Charnay B, Claire M,
349 Hébrard E, Trainer MG. 2016 The Pale Orange Dot: The Spectrum and Habitability of Hazy
350 Archean Earth. *Astrobiology* **16**, 873–899. (doi:10.1089/ast.2015.1422)
- 351 10. Catling DC, Zahnle KJ. 2020 The Archean atmosphere. *Sci Adv* **6**. (doi:10.1126/sciadv.aax1420)
- 352 11. Schirrmeister BE, Gugger M, Donoghue PCJ. 2015 Cyanobacteria and the Great Oxidation Event:
353 Evidence from genes and fossils. *Palaeontology* **58**, 769–785. (doi:10.1111/pala.12178)
- 354 12. Duval S, Baymann F, Schoepp-Cothenet B, Trolard F, Bourrié G, Grauby O, Branscomb E,
355 Russell MJ, Nitschke W. 2019 Fougerite: The not so simple progenitor of the first cells. *Interface*
356 *Focus* **9**, 16–20. (doi:10.1098/rsfs.2019.0063)
- 357 13. Jönsson J, Sherman DM. 2008 Sorption of As(III) and As(V) to siderite, green rust (fougerite) and
358 magnetite: Implications for arsenic release in anoxic groundwaters. *Chem Geol* **255**, 173–181.
359 (doi:10.1016/j.chemgeo.2008.06.036)
- 360 14. Døssing LN, Dideriksen K, Stipp SLS, Frei R. 2011 Reduction of hexavalent chromium by ferrous
361 iron: A process of chromium isotope fractionation and its relevance to natural environments. *Chem*
362 *Geol* **285**, 157–166. (doi:10.1016/j.chemgeo.2011.04.005)
- 363 15. Choi J, Batchelor B, Won C, Chung J. 2012 Nitrate reduction by green rusts modified with trace
364 metals. *Chemosphere* **86**, 860–865. (doi:10.1016/j.chemosphere.2011.11.035)
- 365 16. Etique M, Zegeye A, Grégoire B, Carteret C, Ruby C. 2014 Nitrate reduction by mixed iron(II-III)
366 hydroxycarbonate green rust in the presence of phosphate anions: The key parameters
367 influencing the ammonium selectivity. *Water Res* **62**, 29–39. (doi:10.1016/j.watres.2014.05.028)
- 368 17. Onoguchi A, Granata G, Haraguchi D, Hayashi H, Tokoro C. 2019 Kinetics and mechanism of
369 selenate and selenite removal in solution by green rust-sulfate. *R Soc Open Sci* **6**.
370 (doi:10.1098/rsos.182147)
- 371 18. Buessecker S, Imanaka H, Ely T, Hu R, Romaniello SJ, Cadillo-Quiroz H. 2022 Mineral-catalysed
372 formation of marine NO and N₂O on the anoxic early Earth. *Nat Geosci* **15**, 1056–1063.
373 (doi:10.1038/s41561-022-01089-9)
- 374 19. Usman M, Byrne JM, Chaudhary A, Orsetti S, Hanna K, Ruby C, Kappler A, Haderlein SB. 2018
375 Magnetite and Green Rust: Synthesis, Properties, and Environmental Applications of Mixed-Valent
376 Iron Minerals. *Chem Rev* **118**, 3251–3304. (doi:10.1021/acs.chemrev.7b00224)
- 377 20. Trolard F, Bourrié G. 2008 *Chapter 5 Geochemistry of Green Rusts and Fougerite. A Reevaluation*
378 *of Fe cycle in Soils*. (doi:10.1016/S0065-2113(08)00405-7)
- 379 21. Zegeye A *et al.* 2012 Green rust formation controls nutrient availability in a ferruginous water
380 column. *Geology* **40**, 599–602. (doi:10.1130/G32959.1)
- 381 22. Farr O, Elzinga EJ, Yee N. 2022 Effect of Ni²⁺, Zn²⁺, and Co²⁺ on green rust transformation to
382 magnetite. *Geochem Trans* **23**, 3. (doi:10.1186/s12932-022-00080-y)
- 383 23. Dodd MS *et al.* 2022 Abiotic anoxic iron oxidation, formation of Archean banded iron formations,
384 and the oxidation of early Earth. *Earth Planet Sci Lett* **584**. (doi:10.1016/j.epsl.2022.117469)
- 385 24. Halevy I, Alesker M, Schuster EM, Popovitz-Biro R, Feldman Y. 2017 A key role for green rust in
386 the Precambrian oceans and the genesis of iron formations. *Nat Geosci* **10**, 135–139.
387 (doi:10.1038/ngeo2878)

- 388 25. Russell M. 2018 Green Rust: The Simple Organizing 'Seed' of All Life? *Life* **8**, 35.
389 (doi:10.3390/life8030035)
- 390 26. Russell MJ. 2023 A self-sustaining serpentinization mega-engine feeds the fougérite nanoengines
391 implicated in the emergence of guided metabolism. *Front Microbiol* **14**.
392 (doi:10.3389/fmicb.2023.1145915)
- 393 27. Barge LM, Flores E, Baum MM, Velde DGV, Russell MJ. 2019 Redox and pH gradients drive
394 amino acid synthesis in iron oxyhydroxide mineral systems. *Proc Natl Acad Sci U S A* **116**, 4828–
395 4833. (doi:10.1073/pnas.1812098116)
- 396 28. Ruby C, Géhin A, Abdelmoula M, Génin JMR, Jolivet JP. 2003 Coprecipitation of Fe(II) and Fe(III)
397 cations in sulphated aqueous medium and formation of hydroxysulphate green rust. *Solid State*
398 *Sci* **5**, 1055–1062. (doi:10.1016/S1293-2558(03)00121-3)
- 399 29. Bocher F, Géhin A, Ruby C, Ghanbaja J, Abdelmoula M, Génin JMR. 2004 Coprecipitation of
400 Fe(II-III) hydroxycarbonate green rust stabilised by phosphate adsorption. *Solid State Sci* **6**, 117–
401 124. (doi:10.1016/j.solidstatesciences.2003.10.004)
- 402 30. Duan Z, Møller N, Greenberg J, Weare JH. 1992 The prediction of methane solubility in natural
403 waters to high ionic strength from 0 to 250°C and from 0 to 1600 bar. *Geochim Cosmochim Acta*
404 **56**, 1451–1460. (doi:10.1016/0016-7037(92)90215-5)
- 405 31. Agnel MI, Grangeon S, Fauth F, Elkaïm E, Claret F, Roulet M, Warmont F, Tournassat C. 2020
406 Mechanistic and Thermodynamic Insights into Anion Exchange by Green Rust. *Environ Sci*
407 *Technol* **54**, 851–861. (doi:10.1021/acs.est.9b05632)
- 408 32. Lee S, Wang C, Chakrapani V. 2023 Spontaneous Unassisted Conversion of CO₂ to Multicarbon
409 (≥ C₂) Liquid Products on Green Rust Mineral. *ChemRxiv* (doi:10.26434/chemrxiv-2023-bch3f)
- 410 33. Erbs M, Hansen HCB, Olsen CE. 1999 Reductive dechlorination of carbon tetrachloride using
411 iron(II) iron(III) hydroxide sulfate (green rust). *Environ Sci Technol* **33**, 307–311.
412 (doi:10.1021/es980221t)
- 413 34. Szécsényi Á, Li G, Gascon J, Pidko EA. 2018 Mechanistic Complexity of Methane Oxidation with
414 H₂O₂ by Single-Site Fe/ZSM-5 Catalyst. *ACS Catal* **8**, 7961–7972.
415 (doi:10.1021/acscatal.8b01672)
- 416 35. Fang L, Xu L, Deng J, Gao S, Huang LZ. 2021 Induced generation of hydroxyl radicals from green
417 rust under oxic conditions by iron-phosphate complexes. *Chemical Engineering Journal* **414**,
418 128780. (doi:10.1016/j.cej.2021.128780)
- 419 36. Li Z, Li M, Tan B, Du N, Zhang Q, Li C, Zhang Y, Li J, Li J. 2022 Green rust (GR) and glucose
420 oxidase (GOX) based Fenton-like reaction: Capacity of sustainable release, promoted conversion
421 of glucose through GOX-iron and pH self-adjustment. *Environ Res* **208**.
422 (doi:10.1016/j.envres.2021.112656)
- 423 37. Hanna K, Kone T, Ruby C. 2010 Fenton-like oxidation and mineralization of phenol using synthetic
424 Fe(II)-Fe(III) green rusts. *Environmental Science and Pollution Research* **17**, 124–134.
425 (doi:10.1007/s11356-009-0148-y)
- 426 38. Matta R, Hanna K, Chiron S. 2008 Oxidation of phenol by green rust and hydrogen peroxide at
427 neutral pH. *Sep Purif Technol* **61**, 442–446. (doi:10.1016/j.seppur.2007.12.005)
- 428 39. Anipsitakis GP, Dionysiou DD. 2004 Radical Generation by the Interaction of Transition Metals
429 with Common Oxidants. *Environ Sci Technol* **38**, 3705–3712. (doi:10.1021/es035121o)

- 430 40. Alshehri A. 2013 Methanol oxidation on transition elements oxides. *PhD Thesis - Cardiff University*
- 431 41. Rabiou AM, Yusuf IM. 2013 Industrial Feasibility of Direct Methane Conversion to Hydrocarbons
432 over Fe-Based Fischer Tropsch Catalyst. *Journal of Power and Energy Engineering* **01**, 41–46.
433 (doi:10.4236/jpee.2013.15006)
- 434 42. Trolard F, Duval S, Nitschke W, Ménez B, Pisapia C, Ben Nacib J, Andréani M, Bourrié G. 2022
435 Mineralogy, geochemistry and occurrences of fougérite in a modern hydrothermal system and its
436 implications for the origin of life. *Earth Sci Rev* **225**. (doi:10.1016/j.earscirev.2021.103910)
- 437 43. Maithreepala RA, Doong RA. 2005 Enhanced dechlorination of chlorinated methanes and ethenes
438 by chloride green rust in the presence of copper(II). *Environ Sci Technol* **39**, 4082–4090.
439 (doi:10.1021/es048428b)
- 440 44. Choi J, Lee W. 2008 Enhanced degradation of tetrachloroethylene by green rusts with platinum.
441 *Environ Sci Technol* **42**, 3356–3362. (doi:10.1021/es702661d)
- 442 45. O’Loughlin EJ, Burris DR. 2022 Reduction of Chlorinated Ethenes by Ag- and Cu-Amended Green
443 Rust. *Minerals* **12**, 138. (doi:10.3390/min12020138)
- 444 46. Yao W, Zhang J, Gu K, Li J, Qian J. 2022 Synthesis, characterization and performances of green
445 rusts for water decontamination: A review. *Environmental Pollution*. **304**.
446 (doi:10.1016/j.envpol.2022.119205)
- 447 47. Huber SG, Kotte K, Schöler HF, Williams J. 2009 Natural abiotic formation of trihalomethanes in
448 soil: Results from laboratory studies and field samples. *Environ Sci Technol* **43**, 4934–4939.
449 (doi:10.1021/es8032605)
- 450 48. Redeker KR, Kalin RM. 2012 Methyl chloride isotopic signatures from Irish forest soils and a
451 comparison between abiotic and biogenic methyl halide soil fluxes. *Glob Chang Biol* **18**, 1453–
452 1467. (doi:10.1111/j.1365-2486.2011.02600.x)
- 453 49. Wittmer J, Bleicher S, Ofner J, Zetzsch C. 2015 Iron(III)-induced activation of chloride from
454 artificial sea-salt aerosol. *Environmental Chemistry* **12**, 461–475. (doi:10.1071/EN14279)
- 455 50. Bahlmann E, Keppler F, Wittmer J, Greule M, Schöler HF, Seifert R, Zetzsch C. 2019 Evidence for
456 a major missing source in the global chloromethane budget from stable carbon isotopes. *Atmos*
457 *Chem Phys* **19**, 1703–1719. (doi:10.5194/acp-19-1703-2019)
- 458 51. Sattler T *et al.* 2019 Natural formation of chloro- and bromoacetone in salt lakes of Western
459 Australia. *Atmosphere (Basel)* **10**. (doi:10.3390/atmos10110663)
- 460 52. Trolard F, Génin J-MR, Abdelmoula M, Bourrié G, Humbert B, Herbillon A. 1997 Identification of a
461 green rust mineral in a reductomorphic soil by Mossbauer and Raman spectroscopies. *Geochim*
462 *Cosmochim Acta* **61**, 1107–1111. (doi:10.1016/S0016-7037(96)00381-X)
- 463 53. Jorand F, Zegeye A, Ghanbaja J, Abdelmoula M. 2011 The formation of green rust induced by
464 tropical river biofilm components. *Science of The Total Environment* **409**, 2586–2596.
465 (doi:10.1016/j.scitotenv.2011.03.030)
- 466 54. Li Q, Fernandez RP, Hossaini R, Iglesias-Suarez F, Cuevas CA, Apel EC, Kinnison DE, Lamarque
467 JF, Saiz-Lopez A. 2022 Reactive halogens increase the global methane lifetime and radiative
468 forcing in the 21st century. *Nat Commun* **13**. (doi:10.1038/s41467-022-30456-8)
- 469 55. Poulton SW, Canfield DE. 2011 Ferruginous conditions: A dominant feature of the ocean through
470 Earth’s history. *Elements* **7**, 107–112. (doi:10.2113/gselements.7.2.107)

- 471 56. Thibon F, Blichert-Toft J, Tsikos H, Foden J, Albalat E, Albarede F. 2019 Dynamics of oceanic iron
472 prior to the Great Oxygenation Event. *Earth Planet Sci Lett* **506**, 360–370.
473 (doi:10.1016/j.epsl.2018.11.016)
- 474 57. Koeksoy E, Sundman A, Byrne JM, Lohmayer R, Planer-Friedrich B, Halevy I, Konhauser KO,
475 Kappler A. 2019 Formation of green rust and elemental sulfur in an analogue for oxygenated ferro-
476 euxinic transition zones of Precambrian oceans. *Geology* **47**, 211–214. (doi:10.1130/G45501.1)
- 477 58. He H, Wu X, Xian H, Zhu J, Yang Y, Lv Y, Li Y, Konhauser KO. 2021 An abiotic source of Archean
478 hydrogen peroxide and oxygen that pre-dates oxygenic photosynthesis. *Nat Commun* **12**.
479 (doi:10.1038/s41467-021-26916-2)
- 480 59. Zhao G, Tan M, Wu B, Zheng X, Xiong R, Chen B, Kappler A, Chu C. 2023 Redox Oscillations
481 Activate Thermodynamically Stable Iron Minerals for Enhanced Reactive Oxygen Species
482 Production. *Environ Sci Technol* (doi:10.1021/acs.est.3c02302)
- 483 60. He H *et al.* 2023 A mineral-based origin of Earth's initial hydrogen peroxide and molecular oxygen.
484 *Proc Natl Acad Sci U S A* **120**. (doi:10.1073/pnas.2221984120)
- 485 61. Huang Q, Jiang S-Y, Pi D-H, Konhauser KO, Wen X-P, Lu L-Y, Yan H. 2023 Thermochemical
486 oxidation of methane by manganese oxides in hydrothermal sediments. *Commun Earth Environ* **4**,
487 224. (doi:10.1038/s43247-023-00891-6)
- 488 62. Wong ML, Charnay BD, Gao P, Yung YL, Russell MJ. 2017 Nitrogen Oxides in Early Earth's
489 Atmosphere as Electron Acceptors for Life's Emergence. *Astrobiology* **17**, 975–983.
490 (doi:10.1089/ast.2016.1473)
- 491 63. Ducluzeau AL, van Lis R, Duval S, Schoepp-Cothenet B, Russell MJ, Nitschke W. 2009 Was nitric
492 oxide the first deep electron sink? *Trends Biochem Sci* **34**, 9–15. (doi:10.1016/j.tibs.2008.10.005)
- 493 64. Barge LM *et al.* 2022 Prebiotic reactions in a Mars analog iron mineral system: Effects of nitrate,
494 nitrite, and ammonia on amino acid formation. *Geochim Cosmochim Acta* **336**, 469–479.
495 (doi:10.1016/j.gca.2022.08.038)
- 496 65. Leung M, Schwieterman EW, Parenteau MN, Fauchez TJ. 2022 Alternative Methylated
497 Biosignatures. I. Methyl Bromide, a Capstone Biosignature. *Astrophys J* **938**, 6.
498 (doi:10.3847/1538-4357/ac8799)
- 499 66. Russell MJ, Nitschke W, Branscomb E. 2013 The inevitable journey to being. *Philosophical*
500 *Transactions of the Royal Society B: Biological Sciences* **368**. (doi:10.1098/rstb.2012.0254)
- 501 67. Nitschke W *et al.* 2022 Aqueous electrochemistry: The toolbox for life's emergence from redox
502 disequilibria. *Electrochemical Science Advances* (doi:10.1002/elsa.202100192)
- 503 68. Branscomb E, Russell MJ. 2018 Frankenstein or a Submarine Alkaline Vent: Who is Responsible
504 for Abiogenesis?: Part 2: As life is now, so it must have been in the beginning. *BioEssays*. **40**.
505 (doi:10.1002/bies.201700182)
- 506 69. Nitschke W, McGlynn SE, Milner-White EJ, Russell MJ. 2013 On the antiquity of metalloenzymes
507 and their substrates in bioenergetics. *Biochim Biophys Acta Bioenerg* **1827**, 871–881.
508 (doi:10.1016/j.bbabi.2013.02.008)
- 509